

UC Irvine

UC Irvine Previously Published Works

Title

Poly-generating closed cathode fuel cell with carbon capture

Permalink

<https://escholarship.org/uc/item/9xv0z2pj>

Authors

McLarty, Dustin
Brouwer, Jack

Publication Date

2014-10-01

DOI

10.1016/j.apenergy.2014.06.011

Copyright Information

This work is made available under the terms of a Creative Commons Attribution License, available at <https://creativecommons.org/licenses/by/4.0/>

Peer reviewed



Poly-generating closed cathode fuel cell with carbon capture



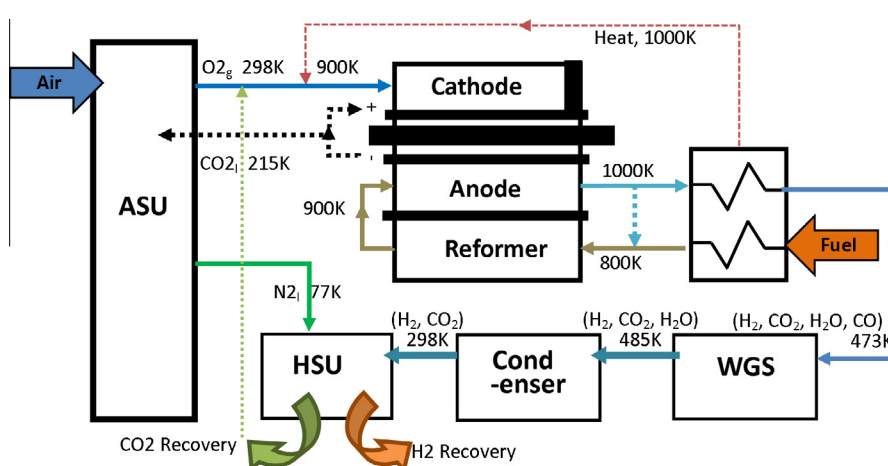
Dustin McLarty, Jack Brouwer*

National Fuel Cell Research Center, University of California, Irvine, CA 92697, USA

HIGHLIGHTS

- A novel poly-generating fuel cell system achieving >80% co-production efficiency.
- Co-production of electricity, hydrogen, heat, and liquefied CO₂, using SOFC or MCFC.
- Closed cathode design utilizing endothermic reforming for stack temperature control.
- Dynamic simulation of stack temperature and control during transient load change.
- Brief economic analysis highlights promising features of co-production benefits.

GRAPHICAL ABSTRACT



ARTICLE INFO

Article history:

Received 14 April 2014

Received in revised form 5 June 2014

Accepted 9 June 2014

Available online 7 July 2014

Keywords:

Solid oxide fuel cell

Poly-generation

Carbon capture

Hydrogen production

Carbon neutral power generation

ABSTRACT

High temperature fuel cells are a promising technology for ultra-low emission power generation. This paper presents a novel poly-generating system capable of greater than 80% (LHV CH₄) co-production efficiency with carbon capture and liquefaction. The proposed system synergistically integrates an air separation unit providing pure oxygen to a fuel cell and liquid nitrogen to a hydrogen separation unit. Both solid oxide and molten carbonate fuel cells may be capable of this integration with additional refrigeration load needed for the molten carbonate system to condense and recirculate carbon dioxide into the cathode stream. Stack temperature control utilizes the endothermic cooling effect of internal fuel reforming. The primary characteristic of the system, converting fuel cell waste heat to produce a secondary fuel (e.g. hydrogen), portends the ultra-high efficiency while enabling additional system design and integration synergies that may reduce complexity, cost, and load following constraints. A unique controller is developed for power and thermal management of a fuel-cooled fuel cell with anode recirculation. A brief economic analysis identifies the potential revenue from each of the four product streams, electricity, hydrogen, heat, and liquid CO₂, and presents a conservative, yet favorable assessment of system costs relative to market electricity and hydrogen fuel prices.

© 2014 Elsevier Ltd. All rights reserved.

1. Introduction

This paper introduces a new high temperature fuel cell system concept which co-produces electricity, heat, hydrogen fuel, and liquefied CO₂ by synergistically integrating a cryogenic air separation

* Corresponding author. Tel.: +1 949 824 7302; fax: +1 949 824 7423.

E-mail addresses: jb@nfcrc.uci.edu, jb@aep.uci.edu, jbrouwer@uci.edu (J. Brouwer).

Nomenclature

ASU	air separation unit	NETL	national energy technology laboratory
EERE	energy efficiency and renewable energy	Oxy-FC	oxygen fed high temperature fuel cell
EOR	enhanced oil recovery	r	anode recirculation ratio
FTE	fuel-to-electric	SECA	solid-state energy conversion alliance
HSU	hydrogen separation unit	SMR	steam methane reformation
MCFC	molten carbonate fuel cell	SOFC	Solid oxide fuel cell
MW	mega-watt	SPU	Single pass fuel utilization
MWh	mega-watt-hour	T	temperature
η	efficiency	U_{fuel}	fuel utilization

unit (ASU), a high temperature fuel cell, and a hydrogen separation unit (HSU). High temperature fuel cells such as molten carbonate and solid oxide technologies readily scale from the residential (1 kW) to industrial sizes (10–100 MW), while current ASU technology is far more effective at industrial scales; see Fig. 4. The HSU separates a dehumidified anode stream consisting primarily of H_2 and CO_2 . Several technologies exist for this separation, but this analysis will consider cryogenic separation using liquid nitrogen co-produced in the ASU with the gaseous oxygen. The ultra-high co-production efficiency and ultra-low greenhouse gas (GHG) and pollutant emissions characterize this transformative technology which could be competitive under present energy rates and regulations while benefiting from stricter future GHG and pollutant emission standards. The ensuing analysis will focus upon natural gas as the energy feedstock, though high methane content biogas (e.g. landfill gas, digester gas) could be readily substituted with the appropriate gas-cleanup technology.

Fig. 1 introduces one potential overall system configuration for the Oxy-FC concept including the three primary components; ASU, high temperature fuel cell, and HSU. The gaseous oxygen and liquid nitrogen produced in the ASU are utilized in the fuel cell and HSU respectively. The fuel cell stack cooling is provided primarily by the endothermic reforming of a hydrocarbon fuel such as natural gas, allowing the cathode to be closed-ended. This increases oxygen partial pressure in the cathode and raises oxygen utilization to 100%. This provides a synergistic benefit to the fuel cell in the form of higher Nernst potential and reduced diffusion losses. The cathode flow rate, reduced by a factor of 20, can be pressurized with minimal parasitic load, providing a further benefit to the fuel cell performance. In the case of a molten carbonate fuel cell (MCFC) a portion of the recovered CO_2 must be recirculated by injecting CO_2 into the ASU oxygen stream at a molar ratio of .5:1 in order to provide the species necessary to form the CO_3^{2-} transport ion. This

has the effect of increases the anode exhaust CO_2 concentration and increasing the parasitic load of the hydrogen separation.

To achieve sufficient stack cooling, excess natural gas is provided to the fuel cell. This serves to increase the hydrogen concentration throughout the anode channels, again benefiting fuel cell performance. The synergies of a thermally integrated fuel reformer are well documented [1]. The excess hydrogen is recovered in the HSU rather than oxidized as in most fuel cell configurations. The final products of this poly-generation concept include electricity from the fuel cell, a small amount of heat from the anode tail gas, hydrogen from the HSU and liquid CO_2 for storage or utilization. Note that the co-production of liquid CO_2 is a byproduct of the cryogenic hydrogen purification. Though less energy intensive means of hydrogen separation are available, namely pressure swing absorption, the inclusion of a cryogenic ASU in the design makes for readily available liquid nitrogen. After the water–gas shift and water condenser, the anode tail gas is composed almost entirely of CO_2 and H_2 . The flow rate of liquid N_2 (boiling temperature of 77.4 K) produced in the ASU for a specified oxygen production is more than sufficient to fully condense the mass flow of CO_2 (boiling temperature of 216.6 K) in the anode tail gas. The aim of this conceptual paper is to introduce the poly-generating Oxy-FC concept, identify the key integration synergies, and estimate the performance potential of the concept.

The closed cathode design of the oxygen blown fuel cell lends itself to several new stack design and manifolding configurations, each with opportunities for innovation. For thermal integration with the fuel reforming process it is important to integrate fuel processing components (e.g. reformer reactor) into the fuel cell stack design. Ideally the fuel processing components would be tailored to locate the bulk of the endothermic reforming process near the areas of high current density, thereby minimizing thermal gradients in the fuel cell stack, reducing mechanical stress and

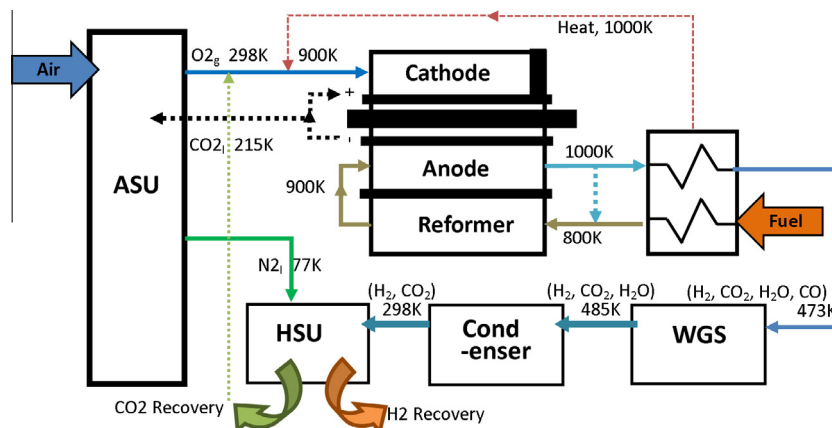


Fig. 1. Poly-generating Oxy-FC system configuration concept and integration schematic.

entropy generation across the cell. The thermodynamic analysis of this novel fuel cell system indicates significant benefit to pressurized operation, which can be achieved with little compression work penalty due to the very low cathode flow rate. As such, stack manifold designs should consider high pressure operation. The need for intricate channel routing across the plate is removed because the cathode channels are supplied with pure O₂ and will not see any concentration drop in the bulk flow, while the anode employs a high degree of recirculation to maintain fuel hydration and therefore also sees minimal reactant concentration drop in the bulk flow. Several existing designs for cylindrical or rectangular planar stack geometries would benefit from the lack of cathode air routing that the current concept allows. Cylindrical designs with a circumferential anode flow pattern would benefit from placing the fuel reformer entrance in direct proximity to the high current region at the anode entrance. Cylindrical designs would also maximize the available volume within a pressurized vessel.

2. Background

Fuel cell technologies have long tantalized engineers with a potential to overcome the Carnot cycle limitations of their heat engine alternatives [2–4]. The fundamental characteristic of a fuel cell is an ion conducting electrolyte which must also be an electronic insulator. The electrolyte separates the oxidation and reduction reactions that would otherwise occur for combustion-based heat engines and produces electricity directly from the chemical potential difference of the separate fuel and oxidant streams. The benefits include the potential for ultra-high efficiency and ultra-low emissions.

A wide search for materials sets that can accomplish the electrochemical reactions and produce electric work has led to a variety of fuel cell types: direct methanol (DMFC), proton exchange membrane (PEM), alkaline (AFC), phosphoric acid (PAFC), molten carbonate (MCFC), and a variety of solid oxide (SOFC) material sets [5]. DMFC technology has been utilized to power handheld electronic devices [6]. AFC's were used aboard space missions beginning in the 60s [7]. PEM fuel cells require relatively pure hydrogen but have found niches in the transportation, material handling and backup power industries [8–10]. PAFC was the first technology commercialized for stationary power, can operate on a range of fossil and bio-fuels, and generate clean electricity at a fuel to electric (FTE) efficiency >40% [11]. MCFC's represent the majority of global fuel cell generating capacity [12] and offer high temperature characteristics amenable to hybridization [13], co-production [14], poly-generation [15], and CO₂ concentration [16,17]. SOFC's have generated substantial interest due to the potential for reduced CO₂ capture penalties in large-scale power production from natural gas [18] or coal gasification [19] SOFC's are considered for their potential low-cost material set, high thermal efficiency, and solid-state structure [20]. As there are typically simpler or less expensive methods of producing electrical power from stored chemical energy (e.g., batteries or combustion), each of these applications utilizes one or more of the unique attributes of fuel cell energy conversion features in addition to its power generating capability. Low emission, low noise, and the mechanical reliability of solid state hardware have been defining characteristics of the technology to-date. These traits remain important, but larger power systems must also capitalize upon the synergies of integrating fuel processing with high temperature fuel cells, the unique arrangement of a fuel cell energy conversion device wherein the fuel and oxidant remain separate (in contrast to combustion systems), or upon the novelty that the large and cumbersome mass of a working fluid and corresponding parasitic burden on the power plant is not required to generate power using this concept.

Stationary fuel cell systems have achieved FTE efficiencies as high as 60% (LHV) on a range of fuels; natural gas, bio-gas, coal-syngas, and hydrogen. Most systems utilize air as the oxidant, although FuelCell Energy® has developed a pure oxygen powered system for undersea applications [21]. High FTE efficiency concepts (60–75% LHV) have been developed including poly-generation [22], FC–GT hybrids [23], coal gasification with carbon capture [24], and supercritical carbon dioxide hybrid cycles [25]. Each of these high temperature fuel cell systems realizes a different degree of thermal integration with, typically, an external fuel processor or gasifier. No system has yet been proposed in which cell cooling is solely accomplished by the endothermic fuel processing reactions. This is the central tenet of the proposed concept which lends itself to further synergistic integration with an ASU and HSU. The current effort will show that the proposed system is capable of achieving similarly high FTE efficiency at large scales while simultaneously recovering high purity hydrogen and liquid CO₂ with minimal parasitic load.

3. Cycle description

The proposed thermodynamic cycle boldly combines the cryogenic temperatures of an air separation unit (ASU) with a high temperature fuel cell and a hydrogen separation unit for energy recovery. The Oxy-FC reforms natural gas into hydrogen, generates electricity, produces both high and low quality waste heat, and generates a liquefied carbon dioxide exhaust. The ASU provides pressurized gaseous oxygen to the fuel cell and liquid nitrogen for the rapid liquefaction of CO₂ from the fuel cell exhaust stream. The resulting poly-generation produces electricity, heat, hydrogen, and liquid CO₂ in various ratios depending upon the fuel cell pressure and power density.

Within the fuel processing sub-system natural gas is hydrated by recirculated anode exhaust to a desirable steam-to-carbon ratio before entering the internal reformer. Within the reformer steam-methane reforming and water-gas-shift chemistry convert the hydrocarbons and steam to a mixture of hydrogen, water, carbon monoxide and carbon dioxide. These reactions are overall endothermic so that they can provide needed cooling to the fuel cell stack. The hydrogen rich mixture is electrochemically oxidized in the anode compartment to produce electricity from the fuel cell. The electrochemical reactions also produce heat, the bulk of which is utilized by the endothermic reforming occurring internal to the fuel cell stack, while the remainder heats the fuel stream. The substantial mass flow and heat capacity of the recirculated anode mixture required to sufficiently hydrate the incoming fuel pre-heats the pipeline gas to temperatures amenable to the fuel reforming process. The non-recirculated anode exhaust stream contains a substantial amount of thermal energy that can be recovered as it is cooled to 420 K prior to the water-gas-shift reactor. A portion of this heat raises the cathode stream temperature above 650 °C. A single or multiple water-gas-shift reactors generate additional hydrogen from the carbon monoxide that remains in the anode exhaust stream. Additional low quality heat can be recovered as the water is condensed out of the exhaust stream. The resulting dry H₂ and CO₂ mixture is refined into two pure streams in the HSU by condensing the CO₂ out of the H₂ gas. The hydrogen stream can be utilized for additional electric power generation, or as a transportation fuel, or sold for industrial applications. There may also be applications for the liquefied CO₂.

4. Thermodynamic analysis

The current thermodynamic analysis was conducted using a spatially resolved dynamic model of system components (e.g. fuel

cell, heat exchangers) as detailed in McLarty et al. [13]. The analysis assumes an SOFC capable of the SECA benchmark performance of 500 mW cm^{-2} at 0.70 V and 80% fuel utilization. The model is developed based on conservations of mass, species, and energy, as well as equations of convective and conductive heat transfer, steam reformation reactions and fuel cell electrochemical reactions. The fuel cell is discretized into equally sized nodes comprised of six control volumes: interconnect plate, internal reformer channels, 2nd interconnect plate, anode gas channels, PEN tri-layer, and cathode gas channels, using a symmetry boundary condition to simulate the stack as a single repeat unit. Only the physical and chemical processes that affect the timescale of interest (i.e., greater than 10 ms) are modeled with dynamic physical expressions. This includes the mass, species and energy balances for the solid and gaseous control volumes (e.g., Eqs. (1)–(3)). The electrochemical kinetics and voltage distribution, modeled by Eqs. (4)–(6), are assumed sufficiently fast to be considered always at steady state with the reactant concentrations determined by Eqs. (1)–(3), (7)–(11), (and) (12).

The reforming and water–gas-shift reactions (Eqs. (7)–(12)) occurring within both the reformer and anode control volumes are described using the kinetics outlined by Drescher and Haberman and Young [26] respectively. Where R_{rf} and R_{sf} represent the forward catalyzed reaction rate constants for the reforming and water gas shift reactions respectively, and AV represents the active surface area to volume ratio which is set to 5×10^5 [27]. The resulting dynamic model includes six temperature states, concentrations of six fuel species (e.g. CH_4 , CO , CO_2 , H_2 , H_2O , and N_2) within the reformer and anode, as well as oxygen within the cathode for a total of 19 states within each node. The repeated cell unit is modeled with a periodic boundary condition to account for heat transfer between adjacent cells. Heat is transferred vertically between each control volume and laterally between nodes. The specific heat transfer expressions are omitted from this model description for brevity. The parameters that are used in the expressions of Eqs. (1)–(12) are presented in Table 1. The dynamic model can be discretized into any number of nodes and can simulate a variety of channel flow directions. An example of resulting steady-state thermal profile is presented in Fig. 2.

Table 1
Geometric, thermal and electrochemical parameters of Oxy-FC.

Component	Parameter	Variable	SOFC	Unit
Geometric	Cell length	L	0.1	m
	Cell width	W	0.1	m
	Plate thickness	t_{BP}	0.006	m
	Anode channel heights	h_i	0.002	m
	Anode channel widths	w_i	0.005	m
	Anode channel wall	t_W	0.002	m
	Membrane thickness	t_M	$18\text{e}-6$	m
	Cathode thickness	t_C	$800\text{e}-6$	m
	Anode thickness	t_A	$50\text{e}-6$	m
	Thermal	PEN density	ρ_{PEN}	375
PEN specific heat		C_{PEN}	800	$\text{J kg}^{-1} \text{K}^{-1}$
PEN conductivity		K_{PEN}	6.19	$\text{W m}^{-1} \text{K}^{-1}$
Plate density		ρ_{BP}	1975	kg m^{-3}
Plate specific heat		C_{BP}	611	$\text{J kg}^{-1} \text{K}^{-1}$
Plate conductivity		k_{BP}	25.23	$\text{W m}^{-1} \text{K}^{-1}$
Electrochemical	Effective oxygen diffusivity	$D_{\text{O}_2, \text{N}_2}^{\text{eff}}$	2×10^{-5}	$\text{m}^2 \text{s}^{-1}$
	Transfer coefficient	α	0.7	
	Exchange current density	j_0	1	A cm^{-2}
	Electrolyte constant	A	13×10^7	$\text{K } \Omega^{-1} \text{m}^{-1}$
	Electrolyte activation energy	ΔG_{act}	100	kJ mole^{-1}

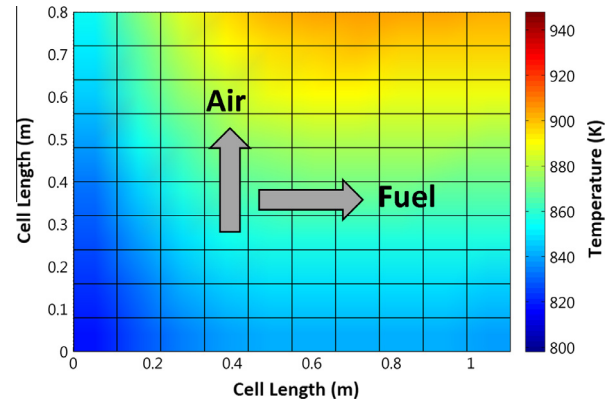


Fig. 2. Steady-state electrolyte temperature profile generated using the current spatially resolved dynamic fuel cell model.

$$\text{Conservation of mass: } \frac{(\dot{n}_{in} - \dot{n}_{out}) \cdot R_u \cdot T}{V} = \frac{dP}{dt} \quad (1)$$

$$\text{Conservation of species: } \frac{R_{ref+Consume} + (\dot{n} \cdot X_i)_{in-out}}{P\sqrt{V}/R_u T} = \frac{dX_i}{dt} \quad (2)$$

$$\text{Conservation of energy: } \frac{\sum Q_i + \dot{q}}{C_p m} = \frac{dT}{dt} \quad (3)$$

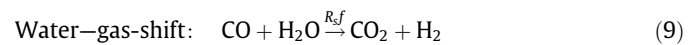
$$\text{Electrochemistry } V_{nernst} = \frac{RT}{2F} \ln \left(\frac{\chi_{\text{H}_2} \cdot \chi_{\text{O}_2}^{1/2}}{\chi_{\text{H}_2\text{O}}} \cdot p^{1/2} \right) \quad (4)$$

$$\eta_{cath} = \frac{RT}{4\alpha F} \ln \left(p \frac{j_l}{j} - \frac{j_l RT t_C}{4FD_{\text{O}_2, \text{N}_2}^{\text{eff}}} \right) \quad (5)$$

$$\eta_{ohm} = j \frac{t_M T}{A e^{-\Delta G_{act}/RT}} \quad (6)$$



$$R_{rf} = \frac{28.52 \cdot P_{\text{CH}_4} P_{\text{H}_2\text{O}} \cdot \exp\left(\frac{-11,000}{RT}\right)}{1 + 16.0 \cdot P_{\text{CH}_4} + 0.143 \cdot P_{\text{H}_2\text{O}} \cdot \exp\left(\frac{39,000}{RT}\right)} \cdot AV \quad (8)$$



$$R_{sf} = k_{sf} \left(P_{\text{H}_2\text{O}} P_{\text{CO}} - \frac{P_{\text{H}_2} P_{\text{CO}_2}}{K_{pS}} \right) \quad (10)$$

$$K_{pS} = 0.0171 \exp \left(-\frac{10,3191}{RT} \right) \quad (11)$$

$$K_{pS} = \frac{\chi_{\text{H}_2} \chi_{\text{CO}_2}}{\chi_{\text{H}_2\text{O}} \chi_{\text{CO}}} \quad (12)$$

Table 2 presents some of the overall system performance results that illustrate the benefits of shifting operation to pure oxygen and pressurization up to 10 atmospheres as proposed in the current Oxy-FC concept. The power and current densities specified correspond to the SECA targets for SOFC technology, however the remaining values such as voltage and fuel utilization would also correspond to a MCFC since the energy balance would be the same. The relative improvement from a baseline air fed MCFC to a pure oxygen/ CO_2 fed MCFC will be slightly less than the improvement shown for the SOFC, and the relative ASU + HSU parasitic will be higher due to the additional CO_2 in the anode exhaust stream.

Table 2

Comparison of the solid state energy conversion alliance (SECA) target SOFC performance to incremental features of the current Oxy-FC concept.

Variable	SECA	Pure O ₂	Pure O ₂ @ 10 atm	Reform cooling	Reform cooling @ 10 atm	Anode Re-circulation	Anode recirculation @ 10 atm	Higher power @ 10 atm
Power (mW cm ⁻²)	500	500	500	500	500	500	500	750
Voltage	0.70	0.817	0.956	0.829	0.954	0.826	0.943	0.9018
Utilization	80%	80%	80%	63.9%	85.3%	70.0%	89.6%	80%
Single pass utilization	80%	80%	80%	63.9%	85.3%	39.7%	79.3%	61.11%
Current (A cm ⁻²)	0.715	0.612	0.523	0.603	.524	0.606	0.530	0.8317
Oxygen (kg _{O2} kW h ⁻¹)	0.427	0.365	0.312	0.360	0.312	0.362	0.316	0.331

The baseline case assumes no anode recirculation and 80% single pass fuel utilization (SPU). While hydrogen is the only fuel constituent that is considered to electrochemically react, the fuel utilization is defined as the electrical current divided by the theoretical molar flow rate of hydrogen if all hydrocarbons and carbon monoxide were oxidized into CO₂ via steam reformation and water-gas-shift. Shifting to pure oxygen increases the voltage from 0.7 to 0.817 V while maintaining equal power density. Thermally balancing the stack heat generation with the fuel reforming requires a 25% increase in fuel flow, reducing fuel utilization from 80% to 63.9%. The additional fuel is reformed to provide cooling to the stack while increasing the average electrochemically active species (e.g. hydrogen) concentration in the bulk anode flow. This illustrates one of the key synergies of co-producing hydrogen as the voltage rises from 0.817 to 0.829 V in response to the higher concentration of electrochemically active species.

Pressurization to 10 atm raises the Nernst potential, and thus increases the voltage further to 0.956 V. At the same level of power generation the higher voltage generates less heat allowing the endothermic reforming to balance the stack heat generation at a SPU of 85.3%. Molten carbonate technology is less amenable to pressurization, thus the analysis will consider an atmospheric case with lower voltage and higher hydrogen co-production.

Pre-heating and humidifying the anode fuel stream requires a substantial amount of thermal energy unless anode recirculation is employed. Anode recirculation simultaneously provides the thermal energy to pre-heat the natural gas and the water vapor for the endothermic reforming and water-gas-shift chemistry. Previously the anode fuel stream was assumed to be provided at the operating temperature of the fuel cell, and was not responsible for any of the stack cooling. With recirculation a thermal gradient is introduced into the anode channels and the fuel stream heat capacity is responsible for a portion of the stack cooling that was otherwise met through endothermic reforming. Anode recirculation also modifies the bulk-stream concentration of reactants. The combined impact on the thermally balanced oxygen-fed SOFC is an increase of global fuel utilization to 70% and a reduction in SPU to 40% when pressure is 1 atm. When pressurized to 10 atm thermal equilibrium is achieved at a global utilization of 89.6% and a SPU of 79.3%. Interestingly the SPU for the pressurized system is very similar to the reference SECA case, though the voltage is considerably higher. An alternative and perhaps more economically viable condition at which the Oxy-FC could operate would be that of an increased power density and lower voltage. Raising the power output to 750 mW cm⁻² lowers fuel utilization to 80% and SPU to 61.11%. This condition has the advantage of producing 50% more power per cell than the reference SECA baseline. A summary of these changes to the overall performance characteristics is presented in Table 2.

The addition of anode recirculation makes the energy flow balance less obvious or intuitive. Fig. 3 presents a Sankey diagram of the energy flow for the final condition of a pressurized SOFC operating at 750 mW cm⁻². One can see the large amount of energy

recirculated with the anode recirculation stream and the multiple energy recovery streams; electricity, hydrogen and heat. The diagram has been normalized to 1 kJ of electric generation.

Table 3 presents a summary of the energy flows for the three operating conditions of interest normalized to 1 kJ of fuel input in order that the numeric values relate closely to thermodynamic efficiency. Heat is recovered in two places, upstream of the water-gas-shift reactor at 150 °C, and in the water condenser at 25 °C.

Complexities arise when defining an efficiency that provides for a fair comparison with alternative systems or configurations of the same concept. First and foremost is the fuel to electric efficiency, which can be determined from the SOFC voltage, the fuel utilization, and the parasitic electric loads of the ASU and HSU. The FTE efficiency of the proposed system could range from as high as 77% (LHV natural gas) to as low as 35% (LHV natural gas) depending upon the system size and operating conditions (e.g., relative amounts of electricity and hydrogen products produced). Co-production efficiency values the additional products (i.e., heat and hydrogen) on an equal energy basis as the primary product, electricity. This metric often belies the true value that a system can produce. Summing the useful products (i.e., electricity, heat, and hydrogen) and assuming an ASU parasitic load equal to 20% of the fuel cell electrical output (a reasonable approximation for a MW scale system as shown in Fig. 4) and heat recovery at 150 °C, we arrive at co-production efficiencies of 84.9%, 82.3%, and 83.7% (LHV natural gas) respectively for the aforementioned three operating conditions. Alternatively we could consider the FTE efficiency if the high temperature heat and recovered hydrogen were utilized to generate additional electricity using a steam turbine (30% efficient) and PEM fuel cell (60% efficient). Applying the same 20% ASU parasitic we arrive at FTE efficiencies of 67.2%, 73.9%, and 71.1% (LHV natural gas) respectively for the 3 operating conditions considered. However, efficient steam generation typically necessitates several MW of steam generation, which would correspond to a >30 MW Oxy-FC system, unless sited with an existing co-generation system. At the very large scale (e.g., 100 MW) FTE efficiency could reach as high as 85% (LHV natural gas) due to the reduced ASU parasitic. Note that in each of these cases the parasitic of CO₂ separation and liquefaction is included.

The parasitic load of the ASU and HSU vary with scale, large systems being more efficient. Fig. 4 presents a summary of performance figures for commercial air separation units. Note the logarithmic scale on the x-axis. The smallest units produce slightly less than 1 ton of pure O₂ per day, enough to supply a 100 kW Oxy-FC system. The inefficiency of the smaller ASU units reduces the performance of this system design for small DG units. A 10 ton per day system could support a 1 MW plant with as little as 20% parasitic load on the electrical output, while the parasitic load dips below 10% as the Oxy-FC plant approaches 100 MW, using ASU system performance noted in the literature [28,29] and manufacturer brochures. The HSU parasitic load is determined from the additional electric power needed to liquefy a portion of the nitrogen in the ASU.

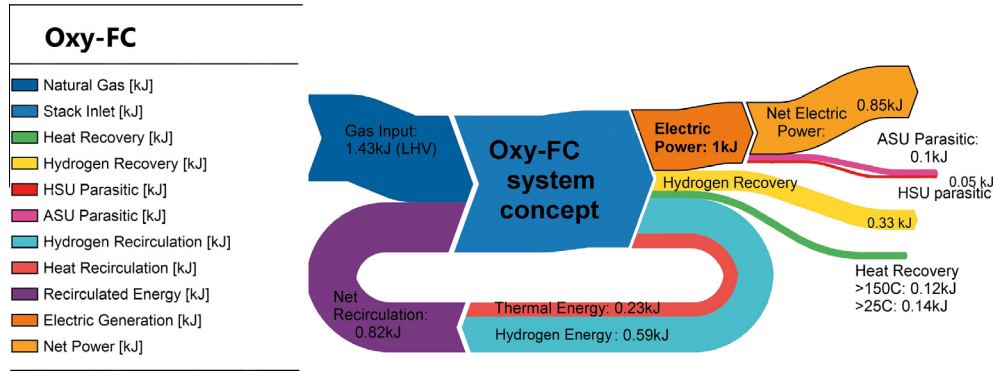


Fig. 3. Sankey diagram of energy flows for the Oxy-FC concept at 10 atm and 750 mW cm⁻².

Table 3
Energy conversion and recovery under different operating conditions.

System	Energy type	Energy recovery @ 1 atm & 500 mW cm ⁻²	Energy recovery @ 10 atm & 500 mW cm ⁻²	Energy recovery @ 10 atm & 750 mW cm ⁻²
Fuel (LHV)	Chemical	1.000	1.000	1.000
SOFC output	Electrical	0.5545	0.8125	0.6983
Heat >150 °C	Thermal	0.0506	0.0492	0.0470
Heat >25 °C	Thermal	0.0797	0.0703	0.0716
H ₂ recovery	Chemical	0.3552	0.1234	0.2312
ASU parasitic ^a	Electrical	-0.0333 to -0.1996	-0.0403 to -0.2438	-0.035 to -0.2095

^a The range in ASU parasitic spans the range of ASU efficiencies from the small (<1 ton/day) to very large (>1000 tons/day) systems.

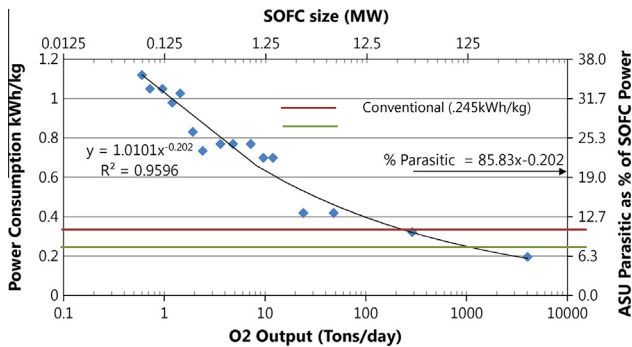


Fig. 4. Summary of ASU performance and parasitic load that it would require from the Oxy-FC system design.

The flow leaving the water condenser is primarily CO₂ and H₂. The flow rate of liquid nitrogen from the ASU can be determined by calculating the cooling requirement necessary to chill this stream below the condensation point of CO₂. Under the operating conditions of design 3 this amounted to an effective refrigeration COP of 2.0. For the remainder of this analysis the HSU parasitic electric load is determined from the CO₂ condensation refrigeration requirement with a COP of 2.0. At larger scales the reduced relative ASU parasitic load and economies of scale for the fuel cell manufacturing, the Oxy-FC concept may compete effectively against established power plant technologies.

5. Part-load analysis

This study notes the unique balancing of power, voltage, and fuel utilization needed to achieve thermal equilibrium in this novel design and operation of a fuel cell system. A unique controller was devised to provide both stack thermal management and rapid load response. Standard FC configurations employing cathode air for cooling are able to independently control for power and fuel utilization by modulating current and fuel flow independently.

The Oxy-FC concept utilizes the fuel flow for cooling, coupling the fuel utilization to the power and requiring both fuel flow and current to be manipulated in tandem. Fig. 5 and Eq. (13) outline a controller for the Oxy-FC concept which manipulates fuel flow and current in response to power and temperature set-points. Two integral and one proportional controller respond to the power, voltage and temperature set-points respectively. In particular, the natural gas flow rate (\dot{n}_{CH_4}) is manipulated to control power while i^* and i are manipulated to control stack voltage and temperature with feedback as shown in Fig. 5. The voltage set-point, determined by Eq. (13), balances the endothermic reforming reactions and exothermic electrochemistry. The heat rates for the three reactions considered (h_{rxn1} , h_{rxn2} , and h_{rxn3}) correspond to hydrogen and oxygen combustion, steam methane reforming and water-gas-shift respectively. Eq. (13) determines the cell operating voltage and assumes that the electrical power output of the stack must be the combustion potential of the portion of fuel participating in

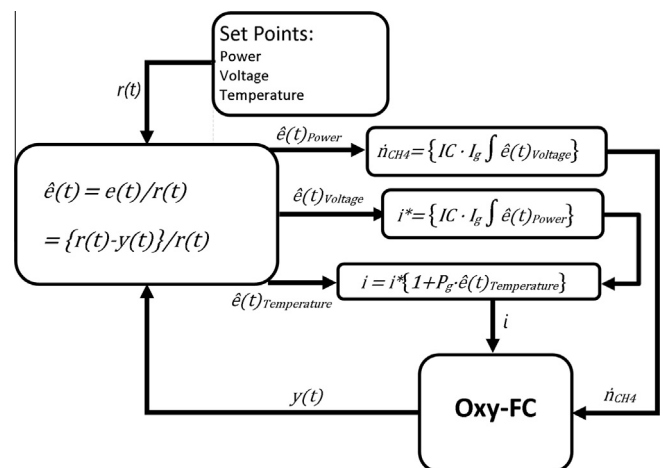


Fig. 5. Oxy-FC part-load and thermal management controller.

the electrochemistry less both the heat transfer to the anode gas and the endothermic reformation process.

$$V \cdot i = \frac{i}{2F} \cdot h_{rxn1} - (\dot{n}C_p \Delta T)_{Anode} - \frac{i \cdot \dot{n}_{CH_4}}{i^* \cdot Cells} \cdot (h_{rxn2} + h_{rxn3}) \quad (13)$$

The sealed cathode compartment enables the oxidant flow control to be completely separate from any other controller. Assuming the oxidant reservoir is kept at higher pressure than the fuel cell, the valve regulating oxygen flow can be controlled to maintain steady pressure in the cathode compartment with occasional purges to remove any buildup of oxygen impurities. Fuel hydration is achieved through anode recirculation. A variable ejector or recirculation blower controls the proportion of anode exhaust entrained in the incoming fuel stream. The proportion of anode exhaust recirculated must be sufficient to both fully hydrate the fuel and pre-heat the incoming natural gas. Assuming an SOFC operating temperature of 800 °C, the anode recirculation will contain sufficient water (e.g., to achieve a steam-to-carbon ratio greater than 2) to avoid coking issues if the mixture of incoming gas (25 °C) and recirculated anode exhaust (800 °C) is sustained >600 °C.

Fig. 6 outlines the part-load performance of the Oxy-FC concept. The voltage reduction at higher power is less than existing fuel cell systems due to increased reactant concentration in the anode and elimination of cathode concentration losses. At part-load the FTE efficiency increases due to reduced current, lower Ohmic losses and less heat generation. Fuel utilization increases in response to maintain the same average fuel cell operating temperature, reducing the amount of recoverable hydrogen. The FTE efficiency reported in this figure assumes a fixed ASU efficiency of 0.4 kW h kg⁻¹ of O₂ generation. This would correspond to an Oxy-FC system of approximately 10 MW. The co-production efficiency for electricity and hydrogen remains nearly constant across the range of operation considered here. This is explained by the notion that net heat generation of the SOFC/fuel reformer combination is small. The reaction enthalpy of the hydrocarbon fuel is nearly completely converted to either electric power or hydrogen fuel. Only the heat escaping with the anode exhaust and the latent heat of vaporization for the water produced is subtracted from the fuel heating value. Operating at a higher power has the primary effect of changing the ratio of electricity production to hydrogen fuel production.

Power tracking, achieved using current control, may be extremely rapid for small perturbations, due to the excess hydrogen present in the anode under typical operating conditions, while larger changes in power are regulated by the fuel valve response and fuel processing transient response. Fuel processing delays in systems with external fuel reformers lead to significant challenges in power tracking [30], but directly integrating the reformer into the stack configuration significantly reduces the fuel transport and processing delay. Challenges associated with fuel starvation

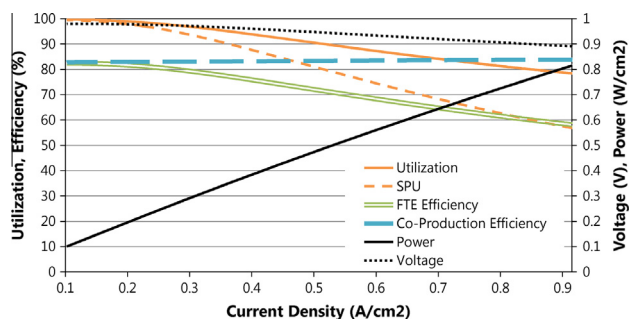


Fig. 6. Part load fuel cell operating conditions and performance characteristics.

during fast ramp-rates are mitigated by the excess hydrogen present in the anode due to recirculation and lower SPU. Therefore, it is expected that a thermally controlled Oxy-FC could respond to load transients quicker than any other high temperature fuel cell due to the lack of external reformer transients, lack of air pre-heating transients and lack of fuel or air blower transients (although the recirculation blower may have similar dynamic response characteristics).

Simulation with fully dynamic, spatially resolved physical models supports this expectation. The results of a rapid, 10 s, load increase from 50% to 100% nominal output for a simulated 1 MW system are presented in Figs. 7 and 8. The step change in power is met in approximately 2 min while the thermal transients persist for slightly more than 5 min. The net power and FTE cannot be accurately portrayed, as the dynamics of the cryogenic air and hydrogen separation units are not simulated. A slight dip appears in the co-production efficiency trend due to the fuel flow delay (~20 s) in reaching the HSU, though a substantially larger delay may occur within the ASU if not buffered by cryogenic storage vessels.

The temperature response increases the spatial temperature gradient by a factor slightly greater than two. Note that the flow configuration simulated has incoming fuel flowing through the reformer channels in the direction opposite of the anode flow. The increased thermal gradient is to be expected as the net power doubles in such a short period of time, and the net heat generation from the electrochemistry more than doubles. The fuel flow increases in proportion to the heat in order to maintain a fixed stack operating temperature, but the additional steam reforming occurring primarily at the fuel entrance (anode exit) requires additional heat transfer from the electrolyte. Controlling the average electrolyte temperature implies that the reformer exit temperature must be cooler as the net heat transfer increases. This subsequently cools the electrolyte near the anode entrance. Increasing the stack power in this configuration has the effect of shifting more of the steam reforming towards the reformer entrance region (anode exit) creating steeper temperature gradients in both the horizontal and vertical planes. The potential exists to control anode recirculation in such a way to mitigate these additional thermal gradients by controlling not to a fixed temperature or humidity ratio, but to a variable set-point, depending upon dynamic operating conditions.

6. Economic analysis

The proposed Oxy-FC system co-produces four useful products from a single natural gas feedstock: electricity, high quality heat, purified hydrogen, and liquefied CO₂. Accurately reflecting the combined value of all four product streams is difficult and compounded by the non-fixed product ratios which vary depending

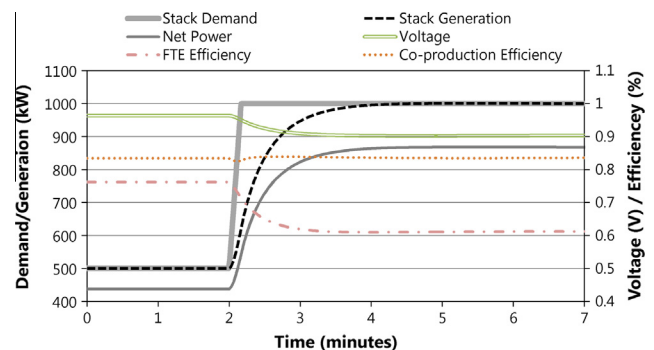


Fig. 7. Simulated Oxy-FC transient response to a rapid load increase from 50% to 100% load for a 1 MW system.

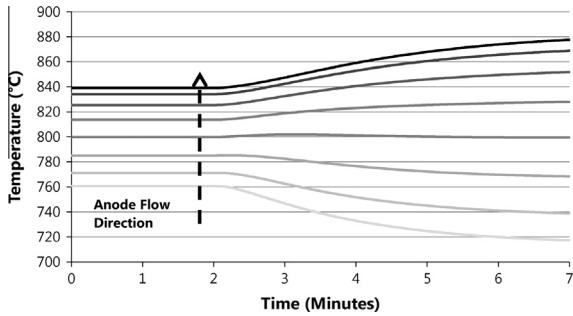


Fig. 8. Spatial temperature response of a simulated 1 MW Oxy-FC to a rapid load increase.

upon the rated capacity and efficiency, the operating net power output conditions, and the recovery effectiveness of the HSU. The value of electricity may also depend upon the local market and the time-of-delivery. The high quality heat could find an application at some distributed power sites, while at a larger scale heat may be wasted or steam generation and bottoming cycles might be considered. A 100 MW Oxy-FC plant might generate an additional 3 MW from steam generation, but at smaller scales the heat may be insufficient to be worth recovering. The hydrogen production could be cost competitive with present commercial hydrogen production via SMR in applications such as oil refining and ammonia production. Current estimates for hydrogen production via SMR range from \$2–5 per kg H₂, while future estimates are as low as \$1.60 per kg H₂ [31].

A simple initial estimate of the cost of carbon-neutral electricity generation using this Oxy-FC concept can be made using the following assumptions:

- Only the electricity and hydrogen outputs will be considered for revenue.
- Hydrogen production is valued at \$2 per kg (consistent with U.S. DOE production cost targets [32]).
- The parasitic electric load of the ASU scales with system capacity as per Fig. 4.
- The Oxy-FC cost is estimated using a system cost learning curve developed by NETL for commercial SOFC technology [33]. The cost estimate assumes an annual manufacturing capacity equal to 10 units at the specified output.
- The ASU cost realizes similar economies of scale and is referenced to a current 40 ton/day system with an installed cost of \$10 million.
- Capital financing is assumed to be 4% over the lifetime of the system, 10 years.
- Natural gas is assumed to be \$4 per MMBTU for an industrial customer.

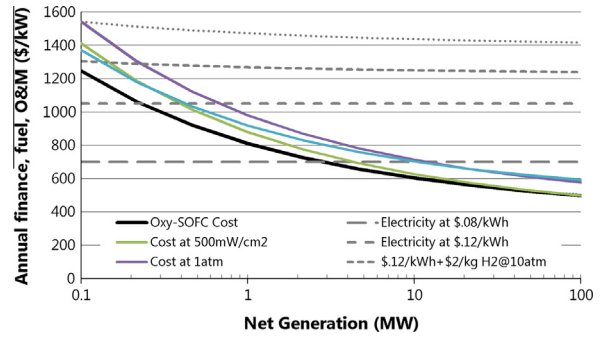


Fig. 9. Annual Oxy-FC cost compared with grid baseline with hydrogen recovery potential.

- Annual operations and maintenance costs are assumed to be a fixed value of \$200 per kW of installed electric capacity.

Fig. 9 presents the costs and recoverable value for the three design operating conditions specified in Table 3. The most economical of the three designs, operation at 10 atm and 750 mW cm⁻², is considered the baseline and presented in greater detail in Table 4. A fourth scenario, with \$6 per MMBTU gas, is also shown. The horizontal dashed lines represent the value of electricity or electricity + hydrogen production displaced by the Oxy-FC generator.

With revenue only from electric generation the Oxy-FC concept reaches parity with \$.08/kWh electricity at a net capacity of 10 MW, 4.5 MW, or 3 MW for system designs 1–3 respectively. System design 3 supplied with \$6 per MMBTU gas reaches parity at 10 MW instead of 3 MW. Revenue from hydrogen generation increases net revenue by 40%, 10%, and 20% for the three designs respectively. As system size increases and operating costs (e.g., fuel costs) dominate, the net savings afforded by the ultra-high efficiency of the Oxy-FC concept become pronounced. At very large scales and with \$4 per MMBTU natural gas a 100 MW Oxy-FC system could produce electricity at \$.03/kWh and hydrogen at \$2/kg. No carbon neutral technology has demonstrated such an ability to be competitive with existing coal fired power costs.

Additional revenue could potentially be realized from the liquefied CO₂ if sold for specialty refrigeration applications, enhanced oil recovery, or sequestered and sold for emissions credits. The value of these applications ranges from \$10 per ton as emissions credits, to \$15–45 per ton for enhanced oil recovery [34], to \$200–\$250 per ton as a specialty refrigerant or beverage addition. The US Department of Energy estimates carbon capture from future fossil power plants to initially cost \$95 per ton with a long term goal of \$44 per ton. For traditional fossil generation sales to enhanced oil recovery would recoup a portion of the carbon capture cost for, but for the Oxy-FC it could provide additional positive revenue. The value of

Table 4
Oxy-FC system concept sizing and cost (\$.08/kWh electricity, \$4/MMBTU gas, \$2/kg H₂, 4% interest financing, \$200/kWh O&M, 10 year life).

Net power (MW)	Rated SOFC (MW)	ASU size ton/day	ASU draw (%)	SOFC cost (\$/kW)	ASU cost (\$/ton)	Baseline grid electricity (\$)	Hydrogen value (\$)	Oxy-FC cost (\$)	Savings (%)
0.10	0.10	1.16	31.38	5067	486,346	70,080	25,361	170,296	-78.43
0.22	0.20	2.35	27.19	4209	403,965	150,983	51,500	305,876	-51.06
0.46	0.40	4.82	23.52	3487	334,664	325,283	105,626	558,444	-29.60
1.00	0.84	9.97	20.31	2883	276,666	700,800	218,393	1,035,406	-12.64
2.15	1.74	20.75	17.52	2379	228,321	1,509,828	454,572	1,948,252	0.82
4.64	3.64	43.42	15.09	1960	188,153	3,252,825	951,349	3,717,667	11.57
10	7.66	91.29	12.98	1614	154,868	7,008,000	2,000,086	7,189,212	20.19
21.5	16.17	192.66	11.17	1327	127,345	15,098,278	4,220,856	14,078,065	27.13
46.4	34.23	407.87	9.60	1090	104,627	32,528,255	8,935,655	27,892,592	32.73
100	72.66	865.77	8.24	895	85,901	70,080,000	18,967,305	55,862,895	37.27

CO₂ emission credits are considerably less than opportunities for enhanced oil recovery if the location allows for EOR. At large scale the waste heat can generate a useful amount of additional electricity, increasing the FTE efficiency and profit margin.

7. Summary and conclusions

This paper presents a novel system integration concept for a high temperature fuel cell. The fuel cell is thermally integrated with the steam methane reforming process for stack temperature control. With thermal management duties removed from the cathode stream (i.e., not using air to cool the fuel cell) a switch to pure oxygen provides several benefits: the option for a sealed (closed end) cathode design, increased voltage potential due to higher reactant concentration, drastically reduced pre-heating heat transfer requirements, reduced compression parasitic, and improved transient response characteristics. A novel thermal controller was used to demonstrate the turndown capability and controllability of an Oxy-FC system. Part-load performance shifted more generation towards electricity with less co-production of hydrogen. Overall FTE efficiency increased while co-production efficiency remained constant. The efficiency of air separation devices suggests that larger systems, >2 MW, are more economically viable, though with hydrogen recovery or in high priced electricity markets an Oxy-FC could be cost-competitive without hydrogen recovery. The additional products of poly-generation, liquid CO₂ and heat, provide only limited additional monetary value, but may become extremely valuable in a carbon-constrained economy.

References

- [1] Winkler Wolfgang. High temperature and solid oxide fuel cells: fundamentals, design and applications. *Thermodynamics* 2003;53–82. <http://dx.doi.org/10.1016/B978-185617387-2/50020-9> [Chapter 3].
- [2] Liebhafsky Herman, Niedrach Leonard. *Fuel cells*. J Franklin Inst 1960;269(4):257–67.
- [3] Bacon FT. The high pressure hydrogen/oxygen fuel cell. In: American Chemical Society Division of Gas and Fuel Chemistry, Atlantic City, 1959, p. 37–69. <<http://web.anl.gov/PCS/acsfuel/preprint%20archive/Files/Volumes/Vol03-3.pdf>>.
- [4] Liebhafsky HA. The fuel cell and the carnot cycle. J Electrochem Soc 1959;106:1068–71.
- [5] Steele CHBrian, Heinzl Angelika. Materials for fuel-cell technologies. *Nature* 2001;414(6861):245–52. <http://dx.doi.org/10.1038/35104620>.
- [6] Sundarrajana Subramanian, Allakhverdiev Suleyman I, Ramakrishna Seeram. Progress and perspectives in micro direct methanol fuel cell. *Int J Hydrogen Energy* 2012;37:8765–86. <http://dx.doi.org/10.1016/j.ijhydene.2011.12.017>.
- [7] Barak M. Fuel cells – present positions and outstanding problems. *Adv Energy Convers* 1966;6:29–55.
- [8] Wipke K, et al., National fuel cell electric vehicle learning demonstration final report, National Renewable Energy Laboratory, Oak Ridge, Technical Report NREL/TP-5600-54860, 2012. <<http://www.nrel.gov/hydrogen/pdfs/54860.pdf>>.
- [9] Todd Ramsden. An evaluation of the total cost of ownership of fuel cell-powered material handling equipment, National Renewable Energy Laboratory, Oak Ridge, Technical Report NREL/TP-5600-56408, 2012. <<http://www.nrel.gov/docs/fy13osti/56408.pdf>>.
- [10] Genevieve Saur, Jennifer Kurtz, Sam Sprik, Todd Ramsden. Fuel cell backup power geographical visualization map, National Renewable Energy Laboratory, Golden, Technical Highlights NREL/FS-5600-56740, 2012. <<http://www.nrel.gov/docs/fy13osti/56740.pdf>>.
- [11] Nymoen Harvard. PAFC demonstration plants in Europe: first results. *J Power Sources* 1994;49:63–76. [http://dx.doi.org/10.1016/0378-7753\(93\)01797-1](http://dx.doi.org/10.1016/0378-7753(93)01797-1).
- [12] Dan Carter, Jonathan Wing. The Fuel Cell Industry Review 2013, Herts, 2013. <<http://www.fuelcelltoday.com>>.
- [13] McLarty Dustin, Brouwer Jack, Samuelsen Scott. A spatially resolved physical model for transient system analysis of high temperature fuel cells. *Int J Hydrogen Energy* 2013;38:7935–46. <http://dx.doi.org/10.1016/j.ijhydene.2013.04.087>.
- [14] Brouwer Jacob. On the role of fuel cells and hydrogen in a more sustainable and renewable energy future. *Curr Appl Phys* 2010;10:S9–S17. <http://dx.doi.org/10.1016/j.cap.2009.11.002>.
- [15] Margalef Pere, Brown Tim M, Brouwer Jacob, Samuelsen Scott. Efficiency comparison of tri-generating HTFC to conventional hydrogen production technologies. *Int J Hydrogen Energy* 2012;37:9853–62. <http://dx.doi.org/10.1016/j.ijhydene.2012.03.099>.
- [16] Jarostaw Milewski, Janusz Lewandowski, Andrzej Miller, Reducing CO₂ emissions from a coal fired power plant by using a molten carbonate fuel cell. In: Proceedings of ASME Turbo Expo 2008: Power for Land, Sea, and Air, vol. 2. 2008, p. 389–95 <<http://dx.doi.org/10.1115/GT2008-50100>>.
- [17] Campanari Stefano, Manzolini Giampaolo, Chiesa Paolo. Using MCFC for high efficiency CO₂ capture from natural gas combined cycles: comparison of internal and external reforming. *Appl Energy* 2013;112:772–83. <<http://dx.doi.org/10.1016/j.apenergy.2013.01.045>>.
- [18] Sung Ku Park, Tong Seop Kim, Sohn Jeong L, Young Duk Lee. An integrated power generation system combining solid oxide fuel cell and oxy-fuel combustion for high performance and CO₂ capture. *Appl Energy* 2011;88:1187–96. <<http://dx.doi.org/10.1016/j.apenergy.2010.10.037>>.
- [19] Siefert Nicholas S. Shawn litster, exergy and economic analyses of advanced IGCC-CCS and IGFC-CCS power plants. *Appl Energy* 2013;107:315–28. <<http://dx.doi.org/10.1016/j.apenergy.2013.02.006>>.
- [20] Minh Nguyen Q. Ceramic fuel cells. *J Am Ceram Soc* 1993;76(3):563–88. <http://dx.doi.org/10.1111/j.1151-2916.1993.tb03645.x>.
- [21] Ghezel-Ayagh Hossein, Jolly Stephen, Sanderson Robert, Hunt Jennifer, Davis Keith E. Hybrid SOFC-battery power system for large displacement unmanned underwater vehicles. *ECS Trans* 2013;51(1):95–101. <http://dx.doi.org/10.1149/05101.0095ecst>.
- [22] Becker WL, Braun RJ, Penev M, Melaina M. Design and technoeconomic performance analysis of a 1 MW solid oxide fuel cell polygeneration system for combined production of heat, hydrogen, and power. *J Power Sources* 2012;200:34–44. <http://dx.doi.org/10.1016/j.jpowsour.2011.10.040>.
- [23] McLarty Dustin, Brouwer Jack, Samuelsen Scott. Fuel cell gas turbine hybrid system design part I: steady state performance. *J Power Sources* 2013;1–9. <http://dx.doi.org/10.1016/j.jpowsour.2013.11.122>.
- [24] Li Mu, Rao Ashok D, Scott Samuelsen G. Performance and costs of advanced sustainable central power plants with CCS and H₂ co-production. *Appl Energy* 2012;91:43–50.
- [25] Sanchez D, Chacartegui R, Munoz de Escalona JM, Munoz A, Sanchez T. Performance analysis of a MCFC & supercritical carbon dioxide hybrid cycle under part load operation. *Int J Hydrogen Energy* 2011;36:10327–36.
- [26] Young JB, Haberman BA. Three-dimensional simulation of chemically reacting gas flows in the porous support structure of an integrated-planar solid oxide fuel cell. *Int J Heat Mass Transfer* 2004;47:3617–29.
- [27] Andersson Martin, Yuan Jinliang, Paradis Bengt Sundén Hedvig. CFD modeling: different kinetic approaches for internal reforming reactions in an anode-supported SOFC. *J Fuel Cell Sci Technol* 2011;8(3).
- [28] Chao Fu, Gundersen Truls. Using exergy analysis to reduce power consumption in air separation units for oxy-combustion processes. *Energy* 2012;44:60–8.
- [29] Chao Fu, Gundersen Truls. Recuperative vapor recompression heat pumps in cryogenic air separation processes. *Energy* 2013;59:708–18.
- [30] Fardadi Mahshid, McLarty Dustin, Jabbari Faryar. Actuator Limitations in Spatial Temperature Control of SOFC. *J Fuel Cell Sci Technol* 2013;10.
- [31] Lipman Timothy. An Overview of Hydrogen Production and Storage Systems with Renewable Hydrogen Case Studies. Montpelier: Clean Energy States Alliance; 2011.
- [32] Office of energy efficiency and renewable energy, fuel cell technologies office multi-year research, development and demonstration plan, US Department Of Energy, Washington DC; 2012.
- [33] Katrina Krulla, Dale Keairns, Arun Iyengar, Dick Newby. Assessment of the distributed generation market potential for solid oxide fuel cells. In: 14th Annual SECA Workshop, Pittsburgh; 2013. <<http://www.netl.doe.gov/publications/proceedings/13/seca/index.html>>.
- [34] Carter LD. United States Carbon Sequestration Council 2011. <http://uscsc.org/educational_papers.asp>.